Mixed Hemi/Ad-Micelle Sodium Dodecyl Sulfate-Coated Magnetic Iron Oxide Nanoparticles for the Efficient Removal and Trace Determination of Rhodamine-B and Rhodamine-6G

ARTICLE *in* ANALYTICAL CHEMISTRY · JULY 2015

Impact Factor: 5.64 · DOI: 10.1021/acs.analchem.5b01676 · Source: PubMed

4 AUTHORS, INCLUDING:

Elias Ranjbari

Tehran University of Medical Sciences

7 PUBLICATIONS **108** CITATIONS

SEE PROFILE

Mohammad Reza Hadjmohammadi

University of Mazandaran

63 PUBLICATIONS **642** CITATIONS

SEE PROFILE

Karolien De Wael

University of Antwerp

93 PUBLICATIONS **584** CITATIONS

SEE PROFILE

analytical chemistry

Article

pubs.acs.org/ac

Mixed Hemi/Ad-Micelle Sodium Dodecyl Sulfate-Coated Magnetic Iron Oxide Nanoparticles for the Efficient Removal and Trace Determination of Rhodamine-B and Rhodamine-6G

Elias Ranjbari,[†,‡] Mohammad Reza Hadjmohammadi,*[,‡] Filip Kiekens,[§] and Karolien De Wael[‡]

[†]AXES, Department of Chemistry, University of Antwerp, Groenenborgerlaan 171, 2020 Antwerp, Belgium

[‡]Department of Analytical Chemistry, Faculty of Chemistry, University of Mazandaran, Babolsar 47416-95447, Iran

[§]Department Pharmaceutics, Campus Drie Eiken, University of Antwerp, Antwerp, Belgium

Supporting Information

ABSTRACT: Mixed hemi/ad-micelle sodium dodecyl sulfate (SDS)-coated magnetic iron oxide nanoparticles (MHAMS-MIONPs) were used as an efficient adsorbent for both removal and preconcentration of two important carcinogenic xanthine dyes named rhodamine-B (RB) and rhodamine-6G (RG). To gain insight in the configuration of SDS molecules on the surface of MIONPs, zeta potential measurements were performed in different [SDS]/[MIONP] ratios. Zeta potential data indicated that mixed hemi/ad-micelle MHAM was formed in [SDS]/[MIONP] ratios over the range of 1.1 to 7.3. Parameters affecting the adsorption of dyes were optimized as removal efficiency by one variable at-a-time and response surface methodology; the obtained removal efficiencies were ~100%. Adsorption kinetic and equilibrium studies, under the optimum condition (pH = 2; amount of MIONPs = 87.15 mg; [SDS]/[MIONP] ratio = 2.9), showed that adsorption of both dyes are based on the pseudo-second-order and the Langmuir isotherm models, respectively. The maximum adsorption capacities for RB and RG were 385 and 323 mg g^{-1}, respectively. MHAMS-MIONPs were also applied for extraction of RB and RG. Under optimum conditions (pH = 2; amount of damped MHAMS-MIONPs = 90 mg; eluent solvent volume = 2.6 mL of 3% acetic acid in acetonitrile), extraction recoveries for 0.5 mg L^{-1} of RB and RG were 98% and 99%, with preconcentration factors of 327 and 330, respectively. Limit of detection obtained for rhodamine dyes were <0.7 ng mL^{-1}. Finally, MHAMS-MIONPs were successfully applied for both removal and trace determination of RB and RG in environmental and wastewater samples.

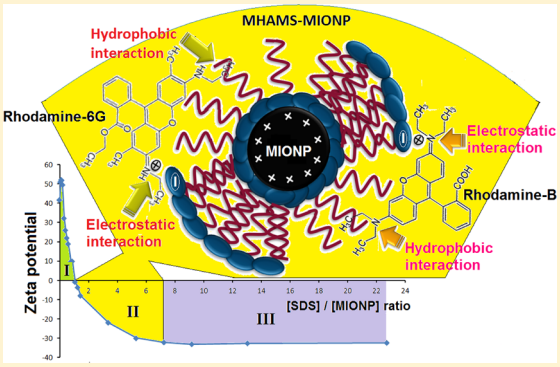

Rhodamine-B (RB) and rhodamine-6G (RG) with multiring aromatic xanthene core planar structure are two of the most popular fluorescent synthetic dyestuffs.[1] RB and RG were used initially as colorant in the textile and food industry, and later, they found wide usage as water tracer, petroleum products dyeing, paper printing, forensic technology, color photography, and cosmetic products. Although the toxicity, mutagenicity, and carcinogenic activities of RG and RB have been experimentally proven,[2−5] these harmful dyes are still illicitly used in some parts of the world, due to their low cost and high efficacy.[6]

Owing to high solubility in water, RB and RG are easily released into the environment, especially into the water resources, during the process of production, manufacture, usage, and disposal of the goods containing these dyes. Releasing these pollutants into the environment, will lead to serious consequences on the health of human beings, plants, animals, and microbes; therefore, making efforts to develop a procedure for removal of these carcinogenic dyes from wastewaters and environmental waters is necessary. Also, providing a sensitive and reliable method for determination of trace amounts of RB and RG for quality control of water samples is inescapable.

Several approaches have been reported in the literature dealing with the removal of rhodamine dyes from aqueous samples either by destruction of the dye molecular structure through photocatalytic degradation,[7] ultrasonic degradation,[8] and sonochemical degradation[9] or by adsorption of the rhodamine molecules at the surface of the adsorbents such as sodium montmorillonite,[10] palm shell-based activated carbon,[11] and walnut shell charcoal.[12] Magnetic nanoparticle-based adsorbents are efficient adsorbents due to their unique advantages over traditional ones; they not only possess high surface area, which can exhibit higher adsorption capacity for analytes, but also have strong magnetic properties which can provide the isolation of sorbents from sample solutions by the application of an external magnetic field; thus, no centrifugation

Received: May 3, 2015
Accepted: July 8, 2015
Published: July 8, 2015

DOI: 10.1021/acs.analchem.5b01676
Anal. Chem. 2015, 87, 7894−7901

of the sample is needed after treatment (in comparison with nonmagnetic adsorbents).[13−15]

Up to now, analysis of RB and RG has been done by various instrumental techniques, such as UV−Vis[16,17] and fluorescence[18] spectrophotometry, high-performance liquid chromatography (HPLC) coupled with UV−Vis detection,[19] and fluorescence detection[20] as well as ultraperformance liquid chromatography tandem mass-spectrometry.[21] However, due to the very low concentration levels of RG and RB in environmental water samples and the complexity of the different matrices, the direct use of spectrometric and chromatographic methods are limited by their selectivity and sensitivity, and that is why the sample preparation and preconcentration of analytes are momentous steps in analytical methods prior to instrumental analysis.

Despite the widespread usage of RB and RG in several industries, only a few reports paid attention to the sample preparation and preconcentration of these carcinogenic compounds aimed to simultaneously determine them.[19,20,22] In previous work,[19] we applied magnetic stirring assisted dispersive liquid−liquid microextraction (MSA-DLLME), based on an extraction solvent with lower density than water, while Xiao et al.[22] determined these dyes by a dispersive liquid−liquid microextraction method based on an extraction solvent with higher density than water. Chiang et al.[20] applied a solid phase extraction (SPE) method based on an HLB-cartridge for the extraction of these two synthetic dyes from surface water and municipal wastewater samples. In recent years, nanoparticles, particularly magnetic nanoparticles (MNPs), have been emerging as a new type of important functional solid phase extraction material. Magnetic nanoparticle-based solid phase extraction (MNP-SPE) consists of two main steps: first, in the adsorption step, analytes are adsorbed on the surface of MNPs, and in the second step, the adsorbed analytes will be desorbed from the surface of MNPs in a suitable solvent for the analysis by an appropriate analytical instrument.

The aim of the ongoing study is utilization of magnetic iron oxide nanoparticles (MIONPs) for both removal and trace determination of RB and RG dyes in wastewater and environmental water samples. Despite the advantages of MIONPs, they are very sensitive when dealing with oxidation and agglomeration; therefore, several organic[23−25] and inorganic[26−28] coatings were applied until now, that in addition to protection of MIONPs, they provide a competent substrate at the surface of the particles for adsorption of analytes. Surface modification of synthesized MIONPs was done by self-assembly of sodium dodecyl sulfate (SDS) as mixed hemi/ad-micelle (MHAM) around MIONPs. To the best of our knowledge, this is the first report of zeta potential studies to gain insight in the configuration of SDS molecules on the surface of MIONPs, although previously some literature reported zeta potential data for SDS coating of alumina[29] and magnetic graphene sheets.[30] The parameters affecting the adsorption of RB and RG by mixed hemi/ad-micelle SDS coated magnetic iron oxide nanoparticles (MHAMS-MIONPs) were optimized, and the best condition was applied to remove the rhodamine dyes from the waste and environmental water samples. Finally, MHAMS-MIONPs were used for MNP-SPE of trace amounts of RB and RG, and after optimization of the parameters affecting extraction, the procedure was successfully applied for the analysis of different water samples.

EXPERIMENTAL SECTION

Chemicals. Standards of RB (≥97%) and RG (99%), methanol (HPLC-grade), ethanol (HPLC-grade), acetone (HPLC-grade), and acetonitrile (HPLC-grade) were purchased from Sigma. The water used for the mobile phase was Milli-Q water. Individual stock solutions of each dye compound were prepared in methanol, and a standard mixture solution of all target compounds was prepared in methanol at a final concentration of 1000 mg L^{-1}. The working solution was prepared by appropriate dilution of the stock solution with distilled water. All of the standard solutions were stored at 4 °C and brought to ambient temperature just prior to use. The instrumentation and operating conditions were described in the Supporting Information.

Preparation of SDS-Coated MIONPs. MIONPs were synthesized by a published coprecipitation method based on formation of iron oxides from aqueous Fe^{2+}/Fe^{3+} salt solutions in the presence of a base;[31] the details of synthesis steps were described in the Supporting Information, as well as characterization of the synthesized MIONPs (Figure S-1). The synthesized MIONPs, which have a large ratio of surface area to volume, tend to agglomerate in order to reduce their surface energy.[32] Modification of the NPs surface is a suitable way to prevent this phenomenon.[33,34] In general, surface modification can be accomplished by physical or chemical adsorption of the desired molecules to coat the surface, depending on the specific applications. After synthesis of MIONPs, hydroxyl groups around nanoparticles lead to an isoelectric point at pH 6.5.[35] Regarding the utilization of SDS (an anionic surfactant) for modification of MIONPs and with respect to the isoelectric point of MIONPs, the modification was performed at pH 5. Then, using a shaker, they were mixed for 3 min to form the suspension of SDS-coated MIONPs. Depending on the amount of surfactant added to MIONPs, three different kinds of SDS-coated MIONPs, including hemimicelle, ad-micelle, and mixed hemi/ad-micelle (MHAM), can be prepared. The main advantage of the MHAM array above the two other arrays is the ability of MHAM to establish both columbic and hydrophobic interactions with a cationic form of RB and RG dyes. In order to achieve MHAMS-MIONPs, the desired ratios of SDS concentration to the MIONP concentration ([SDS]/[MIONP]) were obtained by zeta potential studies.

Experiments for Optimization of Dye Adsorption on the Surface of MHAMS-MIONPs. The adsorption step, which is enforceable to obtain suitable levels in the environmental waters, wastewaters, or factory effluents, is called the removal step. Various parameters affecting the removal of the dye were studied and optimized. Investigation of the pH factor was performed by one variable at a time, and because of the significant interaction, the two other significant factors, i.e., amount of MIONPs and [SDS]/[MIONP] ratio, were optimized by response surface methodology through central composite design (CCD). Optimization studies were carried out according to the following procedure: (1) the pH of 50 mL aqueous solution of the dyes (50 mg L^{-1}) was adjusted to the desired value; (2) the pH of the MIONP suspension (with certain amount of MIONPs) was adjusted to 5; (3) then, a specified amount of SDS was added into the MIONP suspension, and using a shaker, they were mixed for 3 min to form the suspension of SDS-coated MIONPs; (4) the SDS-coated MIONPs were separated from the water and free SDS molecules using a super magnet (1.3 T), and the aqueous phase

DOI: 10.1021/acs.analchem.5b01676
Anal. Chem. 2015, 87, 7894−7901

was poured out; (5) aqueous solution of sample, from step (1), was added to the SDS-coated MIONP, and the suspension was stirred for 5 min, after dye adsorption; (6) MIONPs were separated from the sample solutions using the magnet; (7) the residual dyes concentrations in the supernatant solution were determined by HPLC-Vis using a calibration curve. To compare the different conditions of removal, the removal efficiency (RE%) was applied which can be obtained by the following equation:

$$\mathrm{RE\%} = \frac{C_0 - C_r}{C_0} \times 100 \tag{1}$$

where C_0 and C_r are the initial and residual concentrations of the dye in the solution (mg L^{-1}), respectively.

Experiments for Optimization of Dye Desorption from the Surface of MHAMS-MIONPs. Desorption studies were performed not only to recover the dyes from the adsorbent but also to restore the adsorption capacity of the exhausted adsorbent and to reuse the MIONPs. Furthermore, the desorption process after adsorption is very important for MNP-SPE of trace amounts of dyes in the water samples. In MNP-SPE of RB and RG, the dyes previously adsorbed on the surface of MHAMS-MIONPs were desorbed by a suitable elution solvent. Then, the eluent was completely separated from the adsorbent, using the supermagnet, and it was evaporated to dryness under a gentle stream of nitrogen. The residue was dissolved in 150 μL of water, as injection solvent, and injected into the HPLC using a 10 μL sample loop. In order to investigate the influence of various experimental parameters on the desorption efficiency of RB and RG from the surface of MHAMS-MIONPs, we used extraction recovery % (ER%). The ER% was defined as the percentage of the total analyte (n_0) extracted into the injection solvent (n_{inj}), according to eq 2:

$$\mathrm{ER\%} = \frac{n_{inj}}{n_0} \times 100 = \frac{C_{inj} \times V_{inj}}{C_0 \times V_0} \times 100 \tag{2}$$

where C_{inj} and C_0 are the concentrations of dyes in injection phase and initial concentration of dyes in aqueous sample, respectively. C_{inj} is determined from a calibration curve which was obtained using a direct injection of the standard solutions to the HPLC-vis system. V_{inj} and V_0 are the volumes of injection phase and aqueous sample, respectively.

The preconcentration factor (PF) was defined as the ratio between the analyte concentration in the injection phase (C_{inj}) and the initial concentration of analyte (C_0) in the aqueous sample, as follows:

$$\mathrm{PF} = \frac{C_{inj}}{C_0} \tag{3}$$

The combination of eqs 2 and 3 gives

$$\mathrm{ER\%} = \mathrm{PF} \times \frac{V_{inj}}{V_0} \times 100 \tag{4}$$

Kinetic Experiments. Kinetic studies were performed in the optimum conditions of removal, and at preset time intervals ranging from 1 to 10 min, the samples of 0.5 mL were taken from the solution to analyze the residual rhodamine dye concentration in the solution. The collected kinetic data were analyzed using pseudo-first order (eq 5),[36] pseudo-second order (eq 6),[37] and intraparticle diffusion (eq 7)[38] models to find out the adsorption rate expression:

$$\log(q_e - q_t) = \log q_e - \frac{k_f}{2.303} t \tag{5}$$

$$\frac{t}{q_t} = \frac{1}{k_s q_e^{\,2}} + \frac{1}{q_e} t \tag{6}$$

$$q_t = k_i t^{0.5} \tag{7}$$

where q_t (mg g^{-1}) and q_e (mg g^{-1}) are amount of dye adsorbed at each time and equilibrium and k_f (min^{-1}), k_s (g mg^{-1} min^{-1}), and k_i (mg g^{-1} $min^{-0.5}$) are the rate constants of pseudo-first-order, pseudo-second-order, and intraparticle diffusion models. To select the best model, correlation coefficients (R^2) of models, as a comparative criterion, were applied for comparison. When the R^2 value is close to 1, it means that the experimental data and the model-predicted values are in agreement.

Adsorption Isotherm Studies. The equilibrium adsorption isotherm was determined using 50 mL of the dye solutions with different initial dye concentrations, 50−2000 mg L^{-1}. The time needed to reach the equilibrium condition as determined in equilibrium studies was 4.0 min. The amount of dye adsorbed per unit mass of adsorbent, q_e (mg g^{-1}), was evaluated by the following equation:

$$q_e = \frac{(C_0 - C_e)}{W} \times V \tag{8}$$

where C_0 and C_e (mg L^{-1}) are the initial and equilibrium liquid phase concentrations of the dye in the solution, respectively. W is the weight of dried MHAMS-MIONP, 0.143 g, and V is the volume of the solution, 0.05 L. The q_e obtained by this equation was 17.46 and 17.43 mg g^{-1} for 50 ppm of RB and RG solutions, respectively, which were very close to the amounts (17.51 mg g^{-1} for both dyes) obtained by the slope of the pseudo-second order kinetic model.

The obtained data were compared using three isotherm equations, namely, Langmuir (eq 9),[39] Freundlich (eq 10),[40] and Tempkin (eq 11)[41] adsorption isotherm models.

$$\frac{C_e}{q_e} = \frac{1}{K_L q_{max}} + \frac{1}{q_{max}} C_e \tag{9}$$

$$\log q_e = \log K_F + \frac{1}{n} \log C_e \tag{10}$$

$$q_e = \frac{RT}{b_T} \ln A_T + \left(\frac{RT}{b_T}\right) \ln C_e \tag{11}$$

where q_{max} is the maximum monolayer capacity of the adsorbent (mg g^{-1}), K_L the Langmuir constant (L mg^{-1}), which is related to the adsorption energy, K_F is the Freundlich constant (L g^{-1}), which is an indication of the relative adsorption capacity, n is the heterogeneity factor, which is related to the adsorption intensity, A_T is the Tempkin isotherm equilibrium binding constant (L g^{-1}), R is the universal gass constant (J mol^{-1} K^{-1}), T is the temperature, b_T is the Tempkin isotherm constant, and (RT/b_T) is an indicator of the heat of sorption (J mol^{-1}).

Sample Preparation. The municipal wastewater sample, which was provided from the wastewater treatment plant of Antwerp (Belgium), effluent of University of Antwerp (UA),

DOI: 10.1021/acs.analchem.5b01676
Anal. Chem. 2015, 87, 7894−7901

and Schelde River water were analyzed as the real water samples. All samples were collected into precleaned, light-preserved glass bottles, and each sample was filtered through 0.45 μm membrane filters (Millipore, Bedford, MA). The measurement of the dyes was performed by the standard addition method using calibration curves of 0.001−0.01 mg L^{-1} spiked water samples.

RESULTS AND DISCUSSION

Determining MHAM Condition through Zeta Potential Studies. Zeta potential was measured by Zetasizer (Malvern Instruments Ltd., GB) and through analyzing different suspensions of SDS-coated MIONPs with different ratios of [SDS]/[MIONP]. All suspensions were provided by 1.0×10^{-3} mol L^{-1} NaCl as background electrolyte solution in the absence of target compounds. Figure 1 displays the zeta

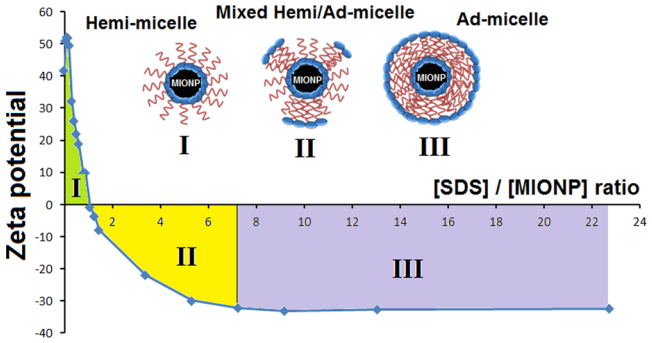

Figure 1. Zeta potential measurements in different [SDS]/[MIONP] ratios.

potential of adsorbent surface versus the [SDS]/[MIONP] ratio. The reported zeta potentials are the average results of five repetitive measurments, and the standard deviation of measurements changed in the range of 2.6−4.5. The zeta potential measurement of bare MIONPs indicated the value of 41.7 mV because of the positive charge of the MIONPs in acidic conditions (pH = 5). By increasing the ratio of [SDS]/[MIONP] up to 1.1, the surface charge of MIONPs was decreased to 0.0; it means that all the MIONPs were covered by a monolayer of SDS molecules which is called the hemimicelle. This monolayer of SDS molecular array enables the adsorbent to make the hydrophobic interaction with adsorbate. The higher concentration of SDS molecules led to the second layer around the MIONPs by hydrophobic interaction of their carbon chain, and the zeta potential values changed to minus values due to the negative charge of the SDS molecules in the second adsorption layer. However, the enhancement of SDS on the surface decreases the tendency of MIONPs for adsorption of more SDS, sterically and electrostatically, so that the slope of depression would be in an exponential manner, insofar as making a plateau in the [SDS]/[MIONP] ratio of about 7.0. The [SDS]/[MIONP] value of 7.3 is the ratio that all the MIONPs were covered by bilayer of SDS molecules, which is called ad-micelle and enables the adsorbent to have only the columbic interaction with adsorbate. After this ratio, the zeta potential was fixed and the concentration of the SDS was increased in aqueous solution. Between the [SDS]/[MIONP] ratios of 1.1 and 7.3, some parts of each MIONP are coated as bilayer and the other parts remain as monolayer; this self-assembly array of SDS molecules around MIONPs is called mixed hemi/ad-micelle (MHAM).

Not only does the MHAM protect the MIONPs chemically and physically, but also this kind of SDS molecular array provides a substrate around the MIONPs, which is able to attract a cationic form of RB and RG electrostatically as well as make a hydrophobic interaction with them; thus, the subsequent experiments were performed using the MHAMS-MIONPs. The size distributions of MIONPs and MHAMS-MIONPs, which were obtained by dynamic light scattering (DLS), as well as their transmission electron microscopy (TEM) were shown in Figures S-2 and S-3, respectively, Supporting Information.

Effect of pH of the Sample Solution. pH of the solution is an important factor in protonation or deprotonation of molecules which are able to be ionized. To attract RB and RG at the negative surface of MHAMS-MIONPs, rhodamine dyes should be in their cationic form. Regarding the acidic dissociation constant, the neutral form of RG converts to its cationic form at pH 6.13 (pK_{aRG} = 6.13),[42] while transformation of RB from zwitterionic form to cationic form will take place at pH 3.2 (pK_{aRB} = 3.2).[43] The experiments depicted that, by decreasing the pH of the sample, the removal efficiency will increase for both RB and RG (Figure S-4, Supporting Information); however, this enhancement is more pronounced for RB, because in pH values greater than 3, the zwitterion of RB can make a repulsion force to the negative charge of the surface of MHAMS-MIONPs. In the case of RG, although increasing the pH to 6 leads to the loss of positive charge and electrostatic interaction, the hydrophobic interaction prevents the sharp decline of removal efficiency. Therefore, a pH value of 2 was selected for all further experiments.

Effect of [SDS]/[MIONP] Ratio and Amount of MIONP. As it was mentioned in the Determining MHAM Condition through Zeta Potential Studies, different ratios of [SDS]/[MIONP] make different kinds of SDS coverage around the MIONPs. On the other hand, the amount of MIONP determines the adsorbent dosage required for the complete removal of rhodamine dyes. In order to obtain maximum removal efficiency with the lowest amount of MIONPs, the effects of [SDS]/[MIONP] ratio and amount of MIONPs were considered, simultaneously. To evaluate the significance of each effect and to estimate the interaction of these two parameters, response surface methodology was applied using a CCD of experiments. On the basis of the CCD, totally, 16 experiments were carried out in a randomized manner in order to minimize the effect of uncontrollable variables (see Table S-1, Supporting Information). As removal of RB and RG needed to be optimized simultaneously and to obtain one quadratic model, multiplication of removal efficiency (MRE) of two compounds was applied to achieve a compromise among the responses of the two considered analytes. The main factors, their symbols, levels, and design matrix are shown in Table S-1, Supporting Information, as well as the response of each run. The variation range of [SDS]/[MIONP] is in the MHAM region. According to the experimental data, a quadratic polynomial model consisting of the main effects ([SDS]/[MIONP] ratio, X_1, and amount of MIONPs, X_2), quadratic effects (X_1^2 and X_2^2), and interaction effects (X_1X_2) was generated (eq 12):

$$\mathrm{MRE} = 0.9331 - 0.0989X_1 + 0.0731X_2 - 0.0632X_1^2 - 0.0409X_2^2 + 0.0613X_1X_2 \quad (12)$$

The obtained data were evaluated by analysis of variance (ANOVA) using STATISTICA 7.0 (Table S-2, Supporting

DOI: 10.1021/acs.analchem.5b01676
Anal. Chem. 2015, 87, 7894−7901

Information). The ANOVA table (Table S-2, Supporting Information) indicated that the model, main effects, quadratic effects, and interaction effects were significant. "Lack of Fit (LOF) p-value" of 0.082121 implies the LOF is not significantly associated with the pure error; furthermore, coefficient of determination, R^2, was 0.98706 which means that the obtained model can explain the variability in response, MRE, very well.[44]

To visualize the relationship between the response and experimental levels of factors, the MRE was mapped against different combinations of two experimental factors in a three-dimensional response surface plot (Figure 2). According to the

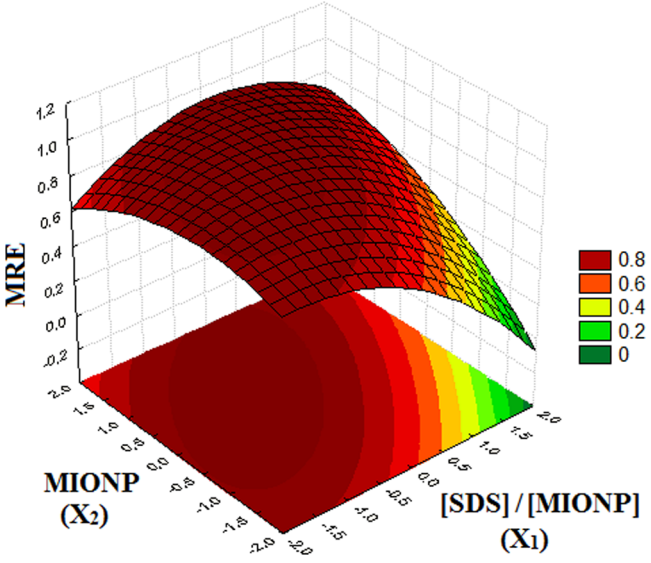

Figure 2. Response surface of the model for simultaneous optimization of [SDS]/[MIONP] ratio (X_1) and amount of MIONPs (X_2).

plotted surface, the recovery reached the maximum when the [SDS]/[MIONP] ratio (X_1) and MIONPs amount (X_2) were around the center point. Finally, the optimum values of [SDS]/[MIONP] ratio (2.9) and MIONP amounts (87.15 mg) for removal of RB and RG were obtained using a grid search program which had been written in Microsoft Office Excel 2010.

To evaluate the optimum condition and its predicted response, 5 replications of the experiments under the predicted optimal conditions were performed, and for both of the dyes, removal efficiency of ~100% was obtained. The relative error in prediction of the removal efficiency was lower than 2.0%. The weight of damped MHAMS-MIONP adsorbent, provided through the optimum condition, was 4.447 g, while it was 0.143 g for dried adsorbent (about 31-fold less than the damped one).

FT-IR Spectroscopy. The efficient adsorption of RB and RG was monitored by FT-IR spectroscopy. The FT-IR of RB, RG, MHAMS-MIONPs, and the adsorbed rhodamine dyes on the surface of MHAMS-MIONPs was shown in Figure S-5, Supporting Information. The obtained results confirmed the adsorption of RB and RG on the surface of MHAMS-MIONPs.

Study of Adsorption Kinetics. The study of adsorption kinetics is important, because it not only is helpful for the prediction of the adsorption rate and equilibrium time but also gives meaningful information for designing and modeling the adsorption processes. Figure S-6a,b, Supporting Information, shows the removal efficiency versus the contact time. The adsorption rate was too fast: the equilibrium state was obtained only in 4.0 min, which is attributed to the large surface area of MHAMS-MIONPs and its two interaction kinds, i.e., columbic and hydrophobic, with the cationic form of RB and RG. Analyzing the kinetic data by pseudo-first order, pseudo-second order, and intraparticle diffusion models (Figure S-6c–h, Supporting Information) indicated that the R^2 values for pseudo-first order and intraparticle diffusion kinetic models were <0.9 and <0.6, respectively. The adsorption data of both of the dyes represented the best fit (R^2 = 1) with the pseudo-second-order kinetic model (Figure S-6e,f, Supporting Information). The obtained value of the amount of dye adsorbed at equilibrium, q_e (mg g^{-1}), for both RB and RG was 17.51 mg g^{-1}.

Study of Adsorption Isotherms. Adsorption isotherm equations express the relation between the dye concentrations in solid phase (the mass of the dye adsorbed at constant temperature per unit mass of the adsorbent) and in liquid phase. The experimental data obtained were fitted to the three different adsorption isotherm models including, Langmuir, Freundlich, and Tempkin models (Table 1). While the

Table 1. Constants and Coefficients of Various Applied Isotherms

		obtained values	
adsorption isotherms	parameters	RB	RG
Langmuir	q_{max} (mg g^{-1})	385	323
	K_L (L mg^{-1})	0.18	−0.25
	R^2	0.9978	0.9963
Freundlich	K_F (L g^{-1})	68.39	57.72
	n	3.26	3.19
	R^2	0.9129	0.8743
Tempkin	A_T (L g^{-1})	15.55	10.18
	RT/b_T	42.94	40.84
	R^2	0.9678	0.9120

Langmuir adsorption isotherm assumes monolayer adsorption of adsorbate onto a homogeneous surface of adsorbent with a finite number of identical sites, the Freundlich model assumes a heterogeneous adsorption of adsorbate onto the surface of adsorbent. Fitting the data in the Langmuir model led to the maximum monolayer capacity, q_{max} (mg g^{-1}), equal to 385 and 323 mg g^{-1}, for RB and RG, respectively; also, fitting the data to the Freundlich model depicted the heterogeneity factors of 3.26 and 3.19. The Tempkin model assumes that heat of adsorption of all molecules in the layer will decrease linearly rather than logarithmically with coverage. The experimental data were fairly well fitted by the Tempkin model; however, the correlation coefficients (tabulated in Table 1) confirmed that the Langmuir model gives better fitting than that of the other models.

Desorption and Regeneration Studies. Desorption of dyes from MHAMS-MIONPs was tested using different kinds of organic solvents (Figure S-7, Supporting Information). The tests were performed by 6 mL of each organic solvent and in three steps (2 mL per step). The results depicted that a solution of acetic acid in acetonitrile (3% v/v) was found to be an effective elution solvent with desorption efficiency of 96% and 98% for RB and RG, respectively, which shows that the adsorption process is reversible.

DOI: 10.1021/acs.analchem.5b01676
Anal. Chem. 2015, 87, 7894–7901

The ability of reusing the MIONPs for removal, in several consecutive adsorption and desorption processes, was tested. After each removal, MIONPs were washed by 5 mL of acetonitrile (without acetic acid) and then by 5 mL of water with pH 5, and after that, 0.25 g SDS was added to the MIONPs prior to the next adsorption−desorption cycle. The results showed that, after 23 cycles, the depression of MRE was only 5%.

Application of MHAMS-MIONPs for the Analysis of Trace Amounts of RB and RG. To apply MHAMS-MIONPs for the trace analysis of RB and RG in real samples, the parameters affecting the ERs% including volume of elution solvent (3% acetic acid in acetonitrile) and amount of sorbent, MHAMS-MIONPs, were optimized, simultaneously, by CCD. Totally, 16 experiments were performed by 0.5 mg L^{-1} aqueous standard solutions of RG and RB in 50 mL (Table S-3, Supporting Information). As the solution of rhodamine dyes in acetonitrile did not show a good chromatographic behavior and in order to preconcentrate the analytes, solvent was evaporated to dryness under a gentle stream of nitrogen; then, the residue was dissolved in 150 μL of water. Obtaining one quadratic model (eq 13) for simultaneous optimization of the ERs of RB and RG, multiplication of ERs (MER) was used (Table S-3, Supporting Information). The ANOVA table (Table S-4, Supporting Information, obtained by the recent experiments, shows that the R^2 value is so satisfying (R^2 = 0.98215). Also, by the help of p-values at 95% confidence levels, it is obvious that the model, main effects, quadratic effects, and interaction effects are significant, while the LOF of the model is not significant.

$$\mathrm{MER} = 0.9515 + 0.0751X_1' + 0.1232X_2' - 0.0469X_1'^2 - 0.0878X_2'^2 - 0.0232X_1'X_2' \quad (13)$$

The visualization of the response (MER) versus different combinations of factor experimental levels (Figure 3), together with the grid search procedure, indicates that the response reaches the maximum when the amount of adsorbent is around the level of 0.6; furthermore, the increase in the elution solvent volume is welcomed. However, the enhancement of this factor greater than the level of 0.6 does not change the recovery of the extraction significantly. Finally, 2.6 mL of extraction solvent volume and 90 mg of the amount of adsorbent, i.e., MHAMS-MIONPs, were determined as the optimum conditions, using the grid search method.

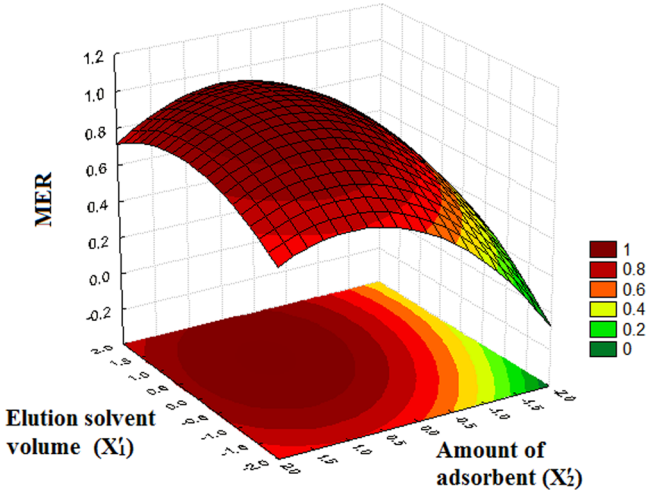

Figure 3. Response surface of the model for simultaneous optimization of volume of elution solvent (X_1') and amount of MHAMS-MIONPs (X_2').

Figure of Merits of the Proposed Extraction Method and Comparison with Previous Works. The analytical features such as extraction recoveries (ERs), preconcentration factors (PFs), relative standard deviations (RSDs), linear ranges (LRs), determination coefficient (R^2), limits of detection (LODs), and limits of quantification (LOQs) for determination of RB and RG were considered. The ERs% for 0.5 mg L^{-1} of RB and RG standard solutions were 98% and 99%, and PFs were 327 and 330, respectively.

RSD values for five replications of extraction were lower than 4.5%. The linearity was observed over the range of 0.001−0.2 mg L^{-1} in the initial solution for both of them, with determination coefficients of 0.9991 for RB and 0.9978 for RG. While the limit of detection and quantification, defined as LOD = $3S_b/m$ and LOQ = $10S_b/m$ (where S_b is the standard deviation of blank and m is the slope of calibration graph after preconcentration), for RB were 0.34 and 1.12 ng mL^{-1} (n = 10), they were 0.21 and 0.69 ng mL^{-1} (n = 10) for RG, respectively.

Only a few methods are available for simultaneous determination of RB and RG.[19,20,22] Table 2 shows the other methods applied for determination of RB and RG, simultaneously. In comparison with previous works, the proposed method shows a very high preconcentration factor, a better LOD, and a desirable linear range for quantitative analysis of RB and RG.

Interference of Ionic Species. The compositions of environmental and wastewater samples are usually complex, and they contain particularly different kinds of ionic species, which may interfere in the extraction and determination process. In order to study the effect of potentially interfering ions on the extraction of 0.5 mg L^{-1} standard solution RB and RG, the tolerance ratio of the method to the different cations (Na^+, K^+, Mg^{2+}, Ca^{2+}, and Fe^{3+}) and anions (NO_3^-, CO_3^{2-}, and PO_4^{3-}) was examined. In Table S-5, Supporting Information, the tolerance ratio shows the ratio of the interfering agent concentration to the concentration of analytes causing a relative error in the MER of less than 10%. The results showed that the ER of the analytes in the presence of interfering ions at the ratios that usually occur in the real samples is quantifiable using the proposed method.

Application of the Proposed Method for Real Samples. To evaluate the applicability of the proposed method in real samples for both removal of RB and RG from the wastewaters and for the determination of trace amounts of these dyes, three different water samples, including a municipal wastewater sample of Antwerp, wastewater of the University of Antwerp, and the Schelde river water sample, were tested. For the aim of removal, all the samples were spiked with RB and RG standards at three levels in 50 mL solutions; subsequently, they were removed using the MHAMS-MIONPs (under optimum conditions: pH of the sample solution = 2; amount of MIONPs = 87.15 mg; [SDS]/[MIONP] ratio = 2.9). Also, for the aim of determination, all the samples were spiked with rhodamine dye standards at five levels in 50 mL solutions and extractions were performed under optimum conditions: pH of the sample solution = 2; amount of damped MHAMS-MIONPs = 90 mg; eluent solvent volume = 2.6 mL, 3% acetic acid in acetonitrile.

DOI: 10.1021/acs.analchem.5b01676
Anal. Chem. 2015, 87, 7894−7901

Table 2. Comparison of the Present Work with Other Methods for Determination of RG and RB, Simultaneously

method	extractant	dye	LOD[a]	LR[a]	R^2	RSD (%)	PF
SPE-HPLC-FLD[b] [20]	methanol + formic acid	RB	0.5×10^{-3}	2−50	0.9950	3	
				50−1000	0.9999		
		RG	0.1×10^{-3}	0.5−20	0.9940	3	
				20−400	0.9994		
DLLME-Vis[22]	chloroform	RB	0.48−1.93	5−450	0.9958−0.9997	<4.7	20
		RG					
MSA-DLLME-Vis[19]	1-octanol	RB	1.23	7.5−1000	0.9999	1.21	48
		RG	1.15	5−1000	0.9999	0.94	46
present work	3% acetic acid in acetonitrile	RB	0.34	0.001−0.2	0.9991	4.3	327
		RG	0.21	0.001−0.2	0.9978	3.9	330

[a]ng mL^{-1}. [b]Fluorescence detection.

The average results of three repetitive analyses of each sample showed REs% of about 100% with RSDs (n = 3) less than 0.2% and the ERs% between 92.25% and 96.38% with RSDs (n = 3) less than 5.0% (Table S-6, Supporting Information). This indicates that, with respect to the complexity of the matrices studied, the values of ERs% and REs%, obtained by the proposed method, are in satisfactory agreement with the added amounts of dyes standards.

CONCLUSION

In this paper, a special kind of SDS-coated MIONPs, i.e., MHAMS-MIONPs, were applied for both removal and determination of RB and RG, as two of the most important xanthine dyes, in wastewater and environmental water samples. The zeta potential measurements were used to determine the [SDS]/[MIONP] ratios at which the SDS molecules are able to form mixed hemi/ad-micelle, MHAM, on the surface of MIONPs. Not only did the MHAM protect the MIONPs chemically and physically, but also this kind of SDS molecular array provided a substrate around the MIONPs which was able to attract the positive form of RB and RG electrostatically and to have hydrophobic interaction with them.

The parameters affecting the adsorption of RB and RG were optimized to obtain the best conditions for their removal. Investigations of the pH factor were performed by one variable at-a-time, and because of the significant interaction, the two other significant factors, i.e., amount of MIONPs and [SDS]/[MIONP] ratios, were optimized by response surface methodology through CCD. Under optimum conditions, the kinetics of the adsorption was investigated, and the obtained results indicated that the pseudo-second-order model provided the best correlation of the adsorption data and the adsorption equilibrium was best defined by the Langmuir isotherm model.

Overall, this paper presents the optimal condition for preparation of MHAMS-MIONPs, as a selective, powerful, and efficient adsorbent with fast adsorption kinetics, good adsorption capacity, and excellent reusability as well as the high chemical stability for removal of rhodamine dyes from water samples. Furthermore, utilization of this adsorbent in MNP-SPE showed sufficient specificity, selectivity, and sensitivity in determination of RB and RG in trace levels for conducting studies on environmental pollution of water samples and quality control of water treatment plants.

ASSOCIATED CONTENT

Supporting Information

Discussion on the synthesis of MIONPs, instrumentation and operating conditions, figure for characterization of synthesized MIONPs (Figure S-1), characterization of MIONPs and MHAMS-MIONPs by DLS and TEM, figure for size distributions of MIONPs (Figure S-2a) and MHAMS-MIONPs (Figure S-2b) by DLS, TEM images of bare MIONPs (Figure S-3a) and MHAMS-MIONPs (Figure S-3a), figure for investigation of the effect of pH of the sample solution on removal efficiency (Figure S-4), description of CCD experiments for simultaneous optimization of [SDS]/[MIONP] and amount of MIONP, a table which shows the main factors, symbols, levels, and design matrix for simultaneous optimization of [SDS]/[MIONP] ratio and amount of MIONPs (Table S-1) with its ANOVA table (Table S-2), figure for FT-IR spectra of RB, RG, MHAMS-MIONP, and MHAMS-MIONPs-RB/RG (Figure S-5) and its description, figure for adsorption kinetic studies (Figure S-6), a figure which indicates the effect of different kinds of elution solvents on recovery of the dyes (Figure S-7), a table which shows main factors, symbols, levels, and design matrix for simultaneous optimization of elution solvent volume and amount of MHAMS-MIONPs (Table S-3) together with the ANOVA table (Table S-4), a table for investigation of interference of ionic species (Table S-5), and a table which represents the removal and determination of RB and RG in waste and environmental water samples (Table S-6). The Supporting Information is available free of charge on the ACS Publications website at DOI: 10.1021/acs.analchem.5b01676.

AUTHOR INFORMATION

Corresponding Author

*Tel/Fax: +981125342350. E-mail: hadjmr@umz.ac.ir.

Notes

The authors declare no competing financial interest.

REFERENCES

(1) Neckers, D. C.; Valdes-Aguilera, O. M. In *Advances in Photochemistry*; Volman, D., Hammond, G. S., Neckers, D. C., Eds.; Wiley: New York, 1993; pp 315−370.

(2) Hood, R. D.; Jones, C. L.; Ranganathan, S. *Teratology* **1989**, *40*, 143−150.

(3) Wuebbles, B. J. Y.; Felton, J. S. *Environ. Mutagen.* **1985**, *7*, 511−522.

(4) Sweatman, T. W.; Seshadri, R.; Israel, M. *Cancer Chemother. Pharmacol.* **1990**, *27*, 205−210.

(5) Thaler, S.; Haritoglou, C.; Choragiewicz, T. J.; Messias, A.; Baryluk, A.; May, C. A.; Rejdak, R.; Fiedorowicz, M.; Zrenner, E.; Schuettauf, F. *Invest. Ophthalmol. Visual Sci.* **2008**, *49*, 2120−2126.

(6) Alesso, M.; Bondioli, G.; Talío, M. C.; Luconi, M. O.; Fernández, L. P. *Food Chem.* **2012**, *134*, 513−517.

(7) Aarthi, T.; Madras, G. *Ind. Eng. Chem. Res.* **2007**, *46*, 7−14.

DOI: 10.1021/acs.analchem.5b01676
Anal. Chem. 2015, 87, 7894−7901

(8) Priya, M. H.; Madras, G. *Ind. Eng. Chem. Res.* **2006**, *45*, 913−921.
(9) Merouani, S.; Hamdaoui, O.; Saoudi, F.; Chiha, M.; Pétrier, C. J. *J. Hazard. Mater.* **2010**, *175*, 593−599.
(10) Selvam, P. P.; Preethi, S.; Basakaralingam, P.; Thinakaran, N.; Sivasamy, A.; Sivanesan, S. *J. Hazard. Mater.* **2008**, *155*, 39−44.
(11) Mohammadi, M.; Hassani, A. J.; Mohamed, A. R.; Najafpour, G. D. J. *J. Chem. Eng. Data* **2010**, *55*, 5777−5785.
(12) Sumanjit; Walia, T. P. S.; Kansal, I. *J. Surf. Sci. Technol.* **2008**, *24*, 179−193.
(13) Travlou, N. A.; Kyzas, G. Z.; Lazaridis, N. K.; Deliyanni, E. A. *Langmuir* **2013**, *29*, 1657−1668.
(14) Mak, S. Y.; Chen, D. H. *Dyes Pigm.* **2004**, *61*, 93−98.
(15) Huang, Y.; Keller, A. A. *ACS Sustainable Chem. Eng.* **2013**, *1*, 731−736.
(16) Biparva, P.; Ranjbari, E.; Hadjmohammadi, M. R. *Anal. Chim. Acta* **2010**, *674*, 206−210.
(17) Pourreza, N.; Rastegarzadeh, S.; Larki, A. *Talanta* **2008**, *77*, 733−736.
(18) Ren, H.; Kulkarni, D. D.; Kodiyath, R.; Xu, W.; Choi, I.; Tsukruk, V. V. *ACS Appl. Mater. Interfaces* **2014**, *6*, 2459−2470.
(19) Ranjbari, E.; Hadjmohammadi, M. R. *Talanta* **2015**, *139*, 216−225.
(20) Chiang, T. L.; Wang, Y. C.; Ding, W. H. *J. Chin. Chem. Soc.* **2012**, *59*, 515−519.
(21) Lu, Q.; Gao, W.; Du, J.; Zhou, L.; Lian, Y. *J. Agric. Food Chem.* **2012**, *60*, 4773−4778.
(22) Xiao, N.; Deng, J.; Huang, K.; Ju, S.; Hu, C.; Liang, J. *Spectrochim. Acta, Part A* **2014**, *128*, 312−318.
(23) Anirudhan, T. S.; Rejeena, S. R.; Binusree, J. *J. Chem. Eng. Data* **2013**, *58*, 1329−1339.
(24) Shen, L.; Laibinis, P. E.; Hatton, T. A. *Langmuir* **1999**, *15*, 447−453.
(25) Harris, L. A.; Goff, J. D.; Carmichael, A. Y.; Riffle, J. S.; Harburn, J. J.; St. Pierre, T. G.; Saunders, M. *Chem. Mater.* **2003**, *15*, 1367−1377.
(26) Chen, C. T.; Chen, Y. C. *Anal. Chem.* **2005**, *77*, 5912−5919.
(27) Lo, C. Y.; Chen, W. Y.; Chen, C. T.; Chen, Y. C. *J. Proteome Res.* **2007**, *6*, 887−893.
(28) Chen, C.-T.; Chen, W. Y.; Tsai, P. J.; Chien, K. Y.; Yu, J. S.; Chen, Y. C. *J. Proteome Res.* **2007**, *6*, 316−325.
(29) Zhao, X.; Li, J.; Shi, Y.; Cai, Y.; Mou, S.; Jiang, G. *J. Chromatogr. A* **2007**, *1154*, 52−59.
(30) Liu, Q.; Shi, J.; Wang, T.; Guo, F.; Liu, L.; Jiang, G. *J. Chromatogr. A* **2012**, *1257*, 1−8.
(31) Huang, C.; Hu, B. *Spectrochim. Acta, Part B* **2008**, *63*, 437−444.
(32) Faraji, M.; Yamini, Y.; Rezaee, M. *J. Iran. Chem. Soc.* **2010**, *7*, 1−37.
(33) Shen, H. Y.; Zhu, Y.; Wen, X. E.; Zhuang, Y. M. *Anal. Bioanal. Chem.* **2007**, *387*, 2227−2237.
(34) Banerjee, S. S.; Chen, D. H. *J. Hazard. Mater.* **2007**, *147*, 792−799.
(35) Zhao, X.; Shi, Y.; Wang, T.; Cai, Y.; Jiang, G. *J. Chromatogr. A* **2008**, *1188*, 140−147.
(36) Ho, Y. S.; McKay, G. *Water Res.* **1999**, *33*, 578−584.
(37) Ho, Y. S.; McKay, G.; Wase, D. A. J.; Forster, C. F. *Adsorpt. Sci. Technol.* **2000**, *18*, 639−650.
(38) Weber, W. J.; Morris, J. C. *J. Sanit. Eng. Div., Am. Soc. Civ. Eng.* **1963**, *89*, 31−60.
(39) Langmuir, I. *J. Am. Chem. Soc.* **1918**, *40*, 1361−1403.
(40) Freundlich, H. M. F. *J. Phys. Chem.* **1906**, *57*, 385−470.
(41) Temkin, M. I.; Pyzhev, V. *Acta Physicochim. URSS* **1940**, *12*, 217−222.
(42) Drug Bank Website; http://www.drugbank.ca/drugs/DB03825.
(43) Mchedlov-Petrossyan, N. O.; Kukhtik, V. I.; Alekseeva, V. I. *Dyes Pigm.* **1994**, *24*, 11−35.
(44) Morgan, E. D. *Chemometrics: Experimental design*; Wiley: New York, 1995.

DOI: 10.1021/acs.analchem.5b01676
Anal. Chem. 2015, 87, 7894−7901

Supporting Information

Mixed hemi/ad-micelle SDS-coated magnetic iron oxide nanoparticles for the efficient removal and trace determination of rhodamine-B and rhodamine-6G

Elias Ranjbari [†,‡], Mohammad Reza Hadjmohammadi [‡,*], Filip Kiekens[§], Karolien De Wael[‡]

[†] AXES, Department of Chemistry, University of Antwerp, Groenenborgerlaan 171, 2020 Antwerp, Belgium

[‡] Department of Analytical Chemistry, Faculty of Chemistry, University of Mazandaran, Babolsar, Iran

[§] Department Pharmaceutics, Campus Drie Eiken, University of Antwerp, Antwerp, Belgium

Corresponding Author:

M. R. Hadjmohammadi (Tel & fax: +981125342350; E-*mail address*: hadjmr@umz.ac.ir)

Abstract

This Supporting Information contains discussion on synthesis of MIONPs, instrumentation and operating conditions, figure for characterization of synthesized MIONPs (Figure S-1), characterization of MIONPs and MHAMS-MIONPs by DLS and TEM, figure for size distributions of MIONPs (Figure S-2a) and MHAMS-MIONPs (Figure S-2b) by DLS, TEM images of bare MIONPs (Figure S-3a), and MHAMS-MIONPs (Figure S-3a), figure for investigation of the effect of pH of the sample solution on removal efficiency (Figure S-2), description of CCD experiments for simultaneous optimization of [SDS]/[MIONP] and amount of MIONP, a table which shows the main factors, symbols, levels and design matrix for simultaneous optimization of [SDS]/[MIONP] ratio and amount of MIONPs by CCD (Table S-1) with its analysis of variance (ANOVA) (Table S-2), figure for FT-IR spectra of RB, RG, MHAMS-MIONP, and MHAMS-MIONPs-RB/RG (Figure S-5) and its description, figure for adsorption kinetic studies (Figure S-3), a figure which indicates the effect of different kinds of elution solvents on recovery of the dyes (Figure S-4), a table which shows main factors, symbols, levels and design matrix for simultaneous optimization of elution solvent volume and amount of MHAMS-MIONPs (Table S-3) together with ANOVA table (Table S-4), a table for investigation of Interference of ionic species (Table S-5), and a table which represents the removal and determination of RB and RG in waste and environmental water samples (Table S-6). This material is available free of charge via the Internet at http://pubs.acs.org.

Synthesis of MIONPs. 5.2 g of $FeCl_3.6H_2O$, 2.0 g of $FeCl_2.4H_2O$ and 0.85 mL of HCl (12 M) were dissolved in 25 mL of deoxygenated mili-Q water in order to prepare Fe^{2+}/Fe^{3+} salt solution which was again degassed with nitrogen gas for 20 min. Meanwhile, 250 mL of a 1.5 mol L^{-1} NaOH solution was degassed (for 15 min) and heated to 80 ° C in a reactor. Then, the Fe^{2+}/Fe^{3+} salt solution was added drop wise using a burette under nitrogen gas protection and vigorous stirring (1200 rpm) by an electronic overhead stirrer (IKA) with a glassware mixer. Whole the process was carried out under nitrogen gas with vigorous stirring and the temperature was fixed by a water bath at 80 °C. The synthesized Fe_3O_4 NPs were stored in its suspension until usage. The concentration of the suspension was 7.0 mg mL^{-1}.

Instrumentation and operating conditions. HPLC experiments were performed by Shimadzu, equipped with a model LC-10AD vp quaternary solvent pump, model 7125i manual Rheodyne injector with a 10 μL sample loop, and UV-Vis detector model SPD 10A vp. Separation was done by an isocratic elution on a C18 (250 × 4.6 mm, 5 μm) column from Waters. Mobile phase was a mixture of acetonitrile and water (60:40, v/v) containing 0.1% phosphoric acid with flow rate of 1.0 mL min-1. All the experiments were done at λmax= 545nm for RB and λmax= 520nm for RG. Adjustment of pH was done by model CyberScan pH 510. To obtain zeta potential of the surface of SDS-coated MIONPs, a Malvern system model ZETASIZER 3000 (Malvern Instruments Ltd., UK) was used. The morphological characterizations have been examined by means of environmental scanning electron microscopy, SEM (Quanta TM 250 FEG, The Netherlands), atomic force microscopy, AFM (Easyscan2 Flex AFM, Switzerland) and transmission electron microscopy, TEM (Zeiss - EM10C, Germany). Fourier transform infrared (FT-IR) spectra of the samples were measured on a pressed pellet with KBr, employing a Tensor 27 spectrometer (Bruker, Germany). X-ray power diffraction (XRPD) was used; it consists of a monochromatic (Ag-Kα) X-ray source of low angular divergence (Incoatec IμS-HB) delivering a focal spot of around 100 μm and a single photon-counting area detector (PILATUS 200K) placed perpendicular to the primary X-ray beam.

Characterization of MIONPs

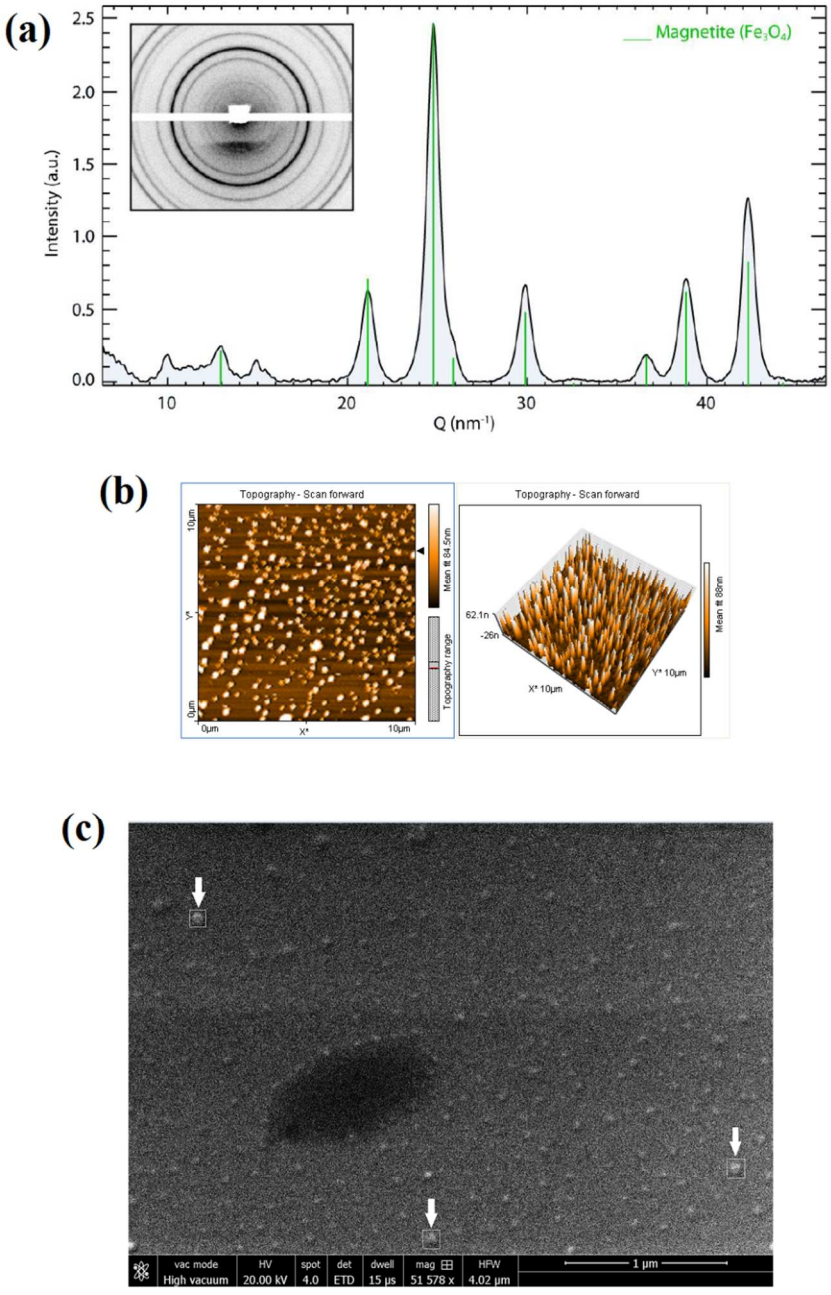

Figure S-1. Characterization of the synthesized MIONPs by: (a) XRD, (b) AFM, and (c) SEM.

The structure of the synthesized MIONPs was primarily characterized by X-ray diffraction (XRD) (Figure S-1a). The observed diffraction peaks are correspond to the crystal planes of (2 2

0), (3 1 1), (4 0 0), (4 2 2), (5 1 1), and (4 4 0), which are matched well with structure of iron oxide nanoparticles in accord with Joint Committee on Powder Diffraction Standards (JCPDS No. 19-629). According to atomic force microscopy (AFM), the average diameter of synthesized MIONPs is about 84 nm (Figure S-1b). Also, scanning electron microscopy (SEM) affirms that the size of particles, respect to the scale bar (1 μm), is below 100 nm (Figure S-1c).

Characterization of MIONPs and MHAMS-MIONPs by DLS and TEM. The size distribution of the MIONPs and MHAMS-MIONPs by DLS (Figure S-2) revealed that the range of size distribution of the MIONPs was approximately narrow, and the size distribution of MHAMS-MIONPs showed wider range. The DLS showed the average size of 151 nm for bare MIONPs with the zeta potential (Zp) of 42 mV. However, DLS analysis of prepared SDS-coated MIONPs with [SDS]/ [MIONP] ratio of 1 and Zp of 0 mV showed the average size of nanoparticles equal to 196 nm, which confirms the immobilization of SDS on the surface of MIONPs. But in the [SDS]/[MIONP] ratios of 3 and 7, the average sizes of particles were 174 and 171 nm, respectively. This depression in the average size can be explained by the Zp of particles. The Zp values at [SDS]/[MIONP] ratios of 3 and 7 were -22 and -32, respectively; thus nanoparticles could be well separated due to the repulsion between SDS molecules in the coating layer.

Also, TEM images of the MIONPs (Figure S-3(a)) and MHAMS-MIONPs (Figure S-3(b)) depict that the particle size of the MHAMS-MIONPs became larger compared to MIONPs, which is attributed to the MHAM coating on MIONPs. However, the hydrodynamic sizes of the particles based on DLS are considerably larger than that observed using TEM. Such differences in the mean diameters have also been observed for other nanomaterials.[S1,S2] As DLS measures hydrodynamic diameter, it provides a fundamentally different measure of particle size than electron microscopy which measures electron diffraction.[S3]

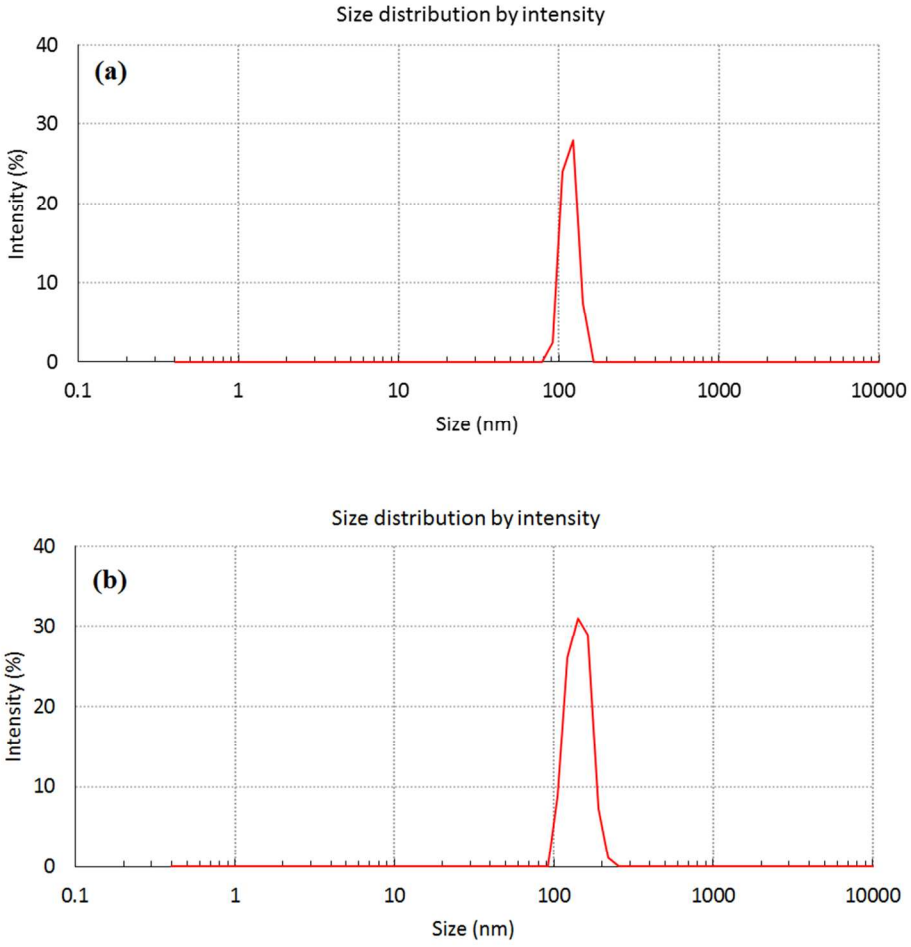

Figure S-2. Size distributions of MIONPs (a) and MHAMS-MIONPs (b) by DLS.

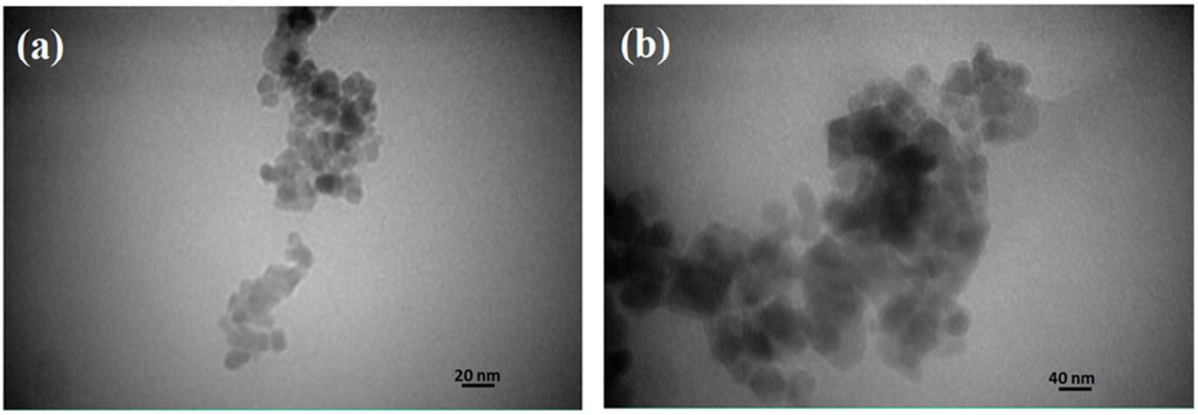

Figure S-3. TEM images of bare MIONPs (a), and MHAMS-MIONPs (b).

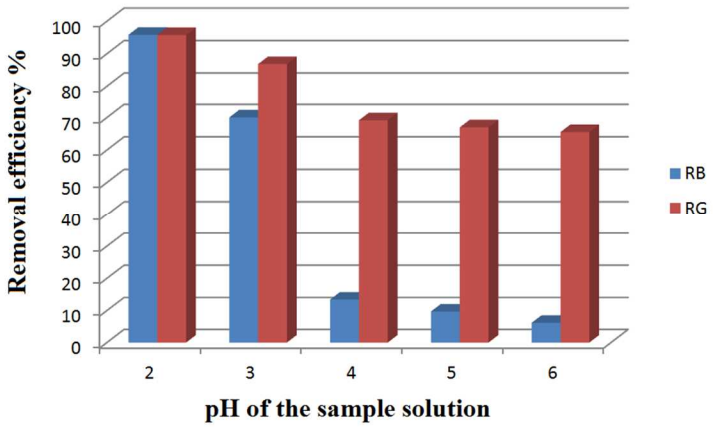

Figure S-4. Effect of pH of the sample solution on removal efficiency of RB and RG ([SDS]/[MIONP] = 2, and amount of MIONPs = 75 mg).

CCD experiments for simultaneous optimization of [SDS]/ [MIONP] and amount of MIONP. The CCD is one of the most common designs used to fit quadratic models and it was first described by Box and Wilson.[S4] A CCD combines 2^f factorial points (N_f) with $2f$ star points (N_α) and one or more central points (N_0) at the center of the experimental region to obtain properties such as rotatability or orthogonality, in order to fit quadratic polynomials.[S5] Therefore, the total number of CCD experiments (N) is determined by the following equation:

$$N = N_f + N_\alpha + N_0 \qquad \text{(S-1)}$$

The star points are located at +α and -α from the center of the experimental domain. The values of α and N_0, needed to ensure orthogonality and rotatability, were calculated equal to ±1.41 and 8 using equations (S-2) and (S-3),[S6] respectively.

$$\alpha = \sqrt[4]{N_f} \qquad \text{(S-2)}$$

$$N_0 = \sqrt{\frac{\sqrt{(N_f + N_\alpha + N_0)N_f} - N_f}{2}} \qquad \text{(S-3)}$$

After performing the experiments, the quadratic polynomial model (equation (S-4)) would be obtained to predict the response of dependent variable:

$$Y = b_0 + \sum_{i=1}^{n} b_i X_i + \sum_{i=1}^{n}\sum_{j=1}^{n} b_{ij} X_i X_j + \sum_{i=1}^{n} b_{ii} X_i^2 \qquad \text{(S-4)}$$

where Y is the dependent variable (or MRE in the present work), X_i is the independent variable, b_0 is the constant coefficient, b_i is the coefficient of linear effect, b_{ij} is the coefficient of interaction effect and b_{ii} is the coefficient of squared effect.

Table S-1. Main factors, symbols, levels and design matrix for simultaneous optimization of [SDS]/[MIONP] ratio and amount of MIONPs by CCD.

Factor	Symbol	Level				
		-1.41	-1	0	1	1.41
[SDS]/[MIONP]	X_1	1	1.87	4	6.13	7
Amount of MIONP	X_2	40	50	75	100	110

Run	X_1	X_2	Multiplication of removal efficiency (MRE)
1	-1	-1	0.9389571
2	-1	1	0.9468780
3	1	-1	0.6049331
4	1	1	0.8581526
5	-1.41	0	0.9290311
6	1.41	0	0.6692931
7	0	-1.41	0.7292308
8	0	1.41	0.9574604
9	0	0	0.9180420
10	0	0	0.9390211
11	0	0	0.9440160
12	0	0	0.9315285
13	0	0	0.9260341
14	0	0	0.9520081
15	0	0	0.9200410
16	0	0	0.9340260

Table S-2. ANOVA table for optimization of [SDS]/[MIONP] ratio and amount of MIONPs.

Source	Sum of Squares	df [a]	Mean Square	F Value	p-value [b] Prob > F	
Model	0.180740	5	0.036148	152.577	0.000000	significant
X_1	0.078043	1	0.078043	567.7263	0.000000	significant
X_1^2	0.031635	1	0.031635	230.1307	0.000001	significant
X_2	0.042605	1	0.042605	309.9282	0.000000	significant
X_2^2	0.013291	1	0.013291	96.6818	0.000024	significant
X_1X_2	0.015043	1	0.015043	109.4292	0.000016	significant
Lack of Fit	0.001407	3	0.000469	3.4115	0.082121	not significant
Pure Error	0.000962	7	0.000137			
Residual	0.002369	10				
Total SS	0.183109	15				

[a] Degree of freedom

[b] A p-value less than 0.05 in the ANOVA table indicates the statistical significance of an effect at 95% confidence level.

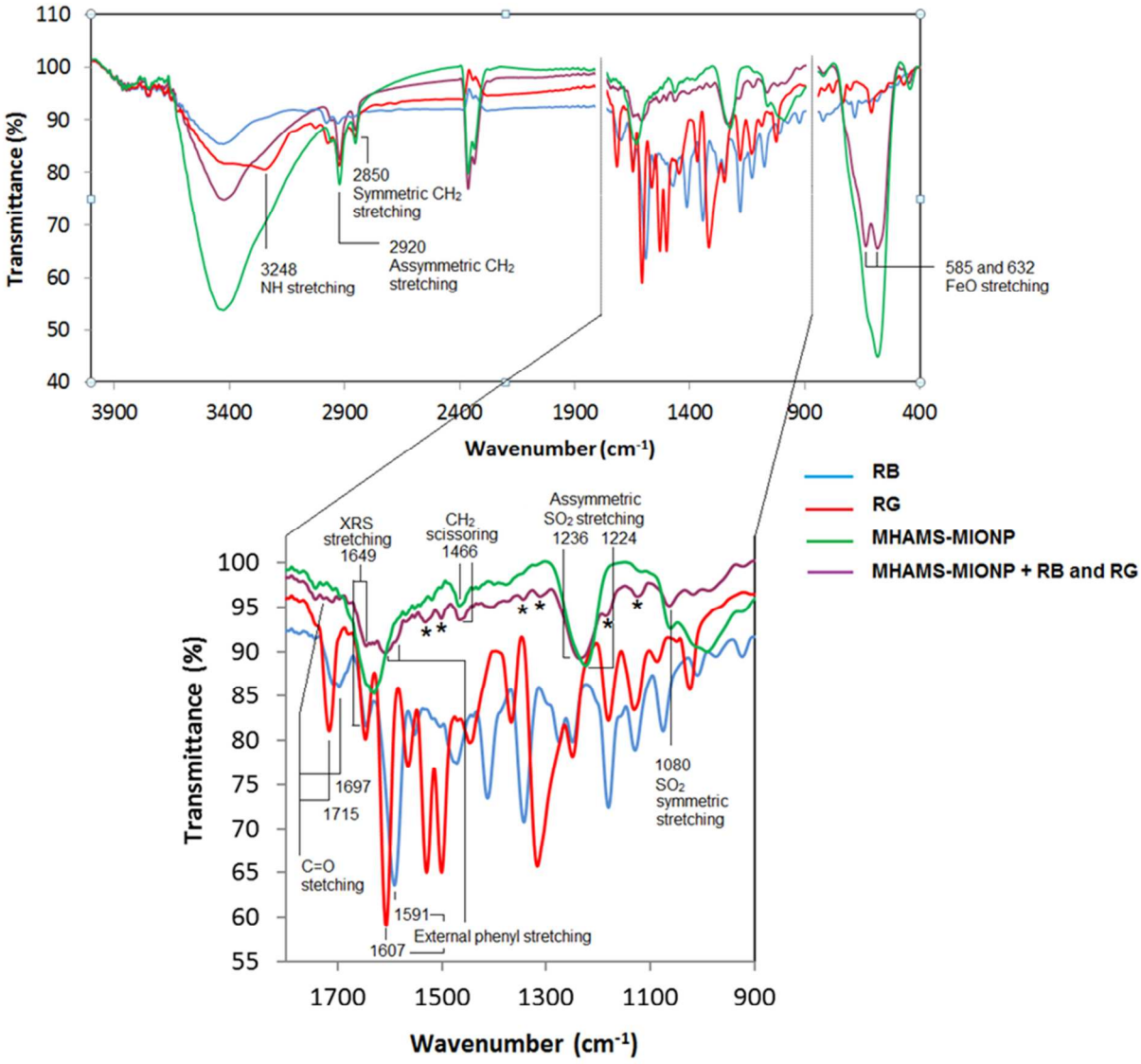

Figure S-5. FT-IR spectra of RB, RG, MHAMS-MIONP, and MHAMS-MIONPs-RB/RG.

The FT-IR spectra of RB, RG, MHAMS-MIONP, and MHAMS-MIONPs-RB/RG were illustrated in Figure S-5. The spectrum in MHAMS-MIONPs-RB/RG is approximately featureless compared with FT-IR spectra of RB, RG, and MHAMS-MIONP, however some transmission bands are recognizable (in the magnified part of Figure S-4). As it can be observed in Figure S-4, the bands at 585 and 632 cm-1 are related to stretching mode of the FeO bond

vibration, which are observable in the spectra of MHAMS-MIONP, and MHAMS-MIONPs-RB/RG. The mode corresponding to the IR band at 1080 cm-1 is assigned to the SO2 symmetric stretching of sulfate group in SDS. The SO2 asymmetric vibrational feature is a combination of several overlapping peaks, and it is generally observed as strong double bands at 1220 and 1250 cm-1;[S7] however, due to the electrostatic interaction of sulfate group with MIONP, the double band was replaced with a single band at 1224 cm-1. After adsorption of RB and RG, this band shifted to 1236 cm-1 which can be attributed to the interactions of sulfate group with RB and RG (such as electrostatic interaction and hydrogen binding). The band at 1466 cm-1 is the indicant of methylene scissoring vibrational mode. The bands at 1591 and 1607 cm-1 are assigned to the skeletal stretching vibration of the external phenyl of RB and RG, respectively.[S8] The FT-IR band at 1649 cm-1 shows the xanthene ring stretching (XRS) of rhodamine dyes. The C=O bond stretching of the carbonyl group of RB and RG is observed at 1697 and 1715 cm-1 and it can be detected as a weak and noisy signal in the MHAMS-MIONPs-RB/RG's spectrum. The two IR bands at 2851 and 2919 cm-1 are attributed to the symmetric and asymmetric CH2 stretching bands. The NH stretching band at 3248 cm-1 was disappeared in the MHAMS-MIONPs-RB/RG's spectrum; however the other bands of RB and RG are observable in the spectrum of MHAMS-MIONPs-RB/RG (marked by asterisk). Therefore, the obtained results confirmed the adsorption of RB and RG on the surface of MHAMS-MIONPs.

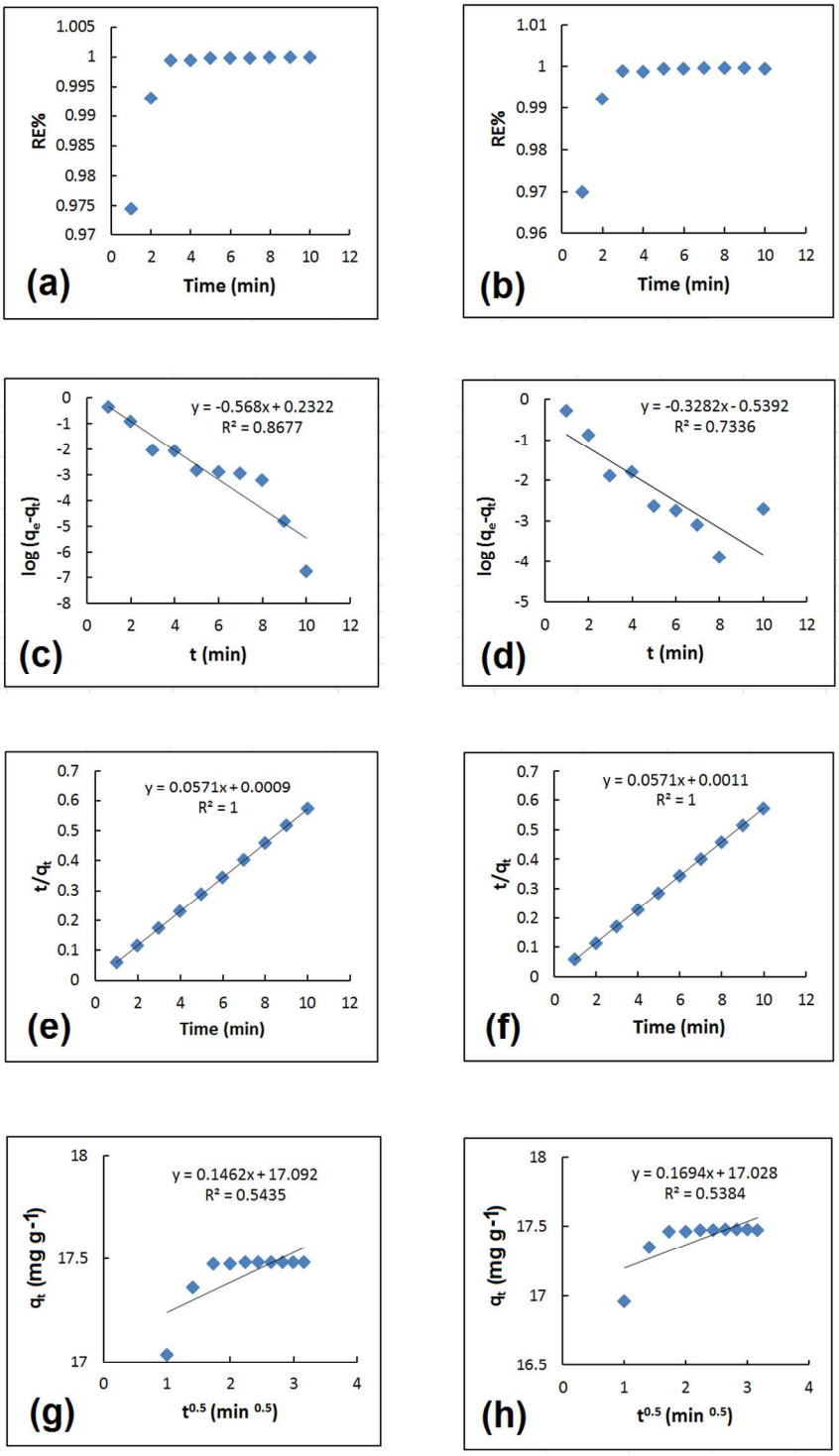

Figure S-6. Adsorption kinetic studies: Influence of contact time on removal efficiency of RB (a); influence of contact time on removal efficiency of RG (b); pseudo-first order model for RB

(c); pseudo-first order model for RG (d); pseudo-second order model for RB (e); pseudo-second order model for RG (f); intra-particle diffusion model for RB (g); intra-particle diffusion model for RB (h).

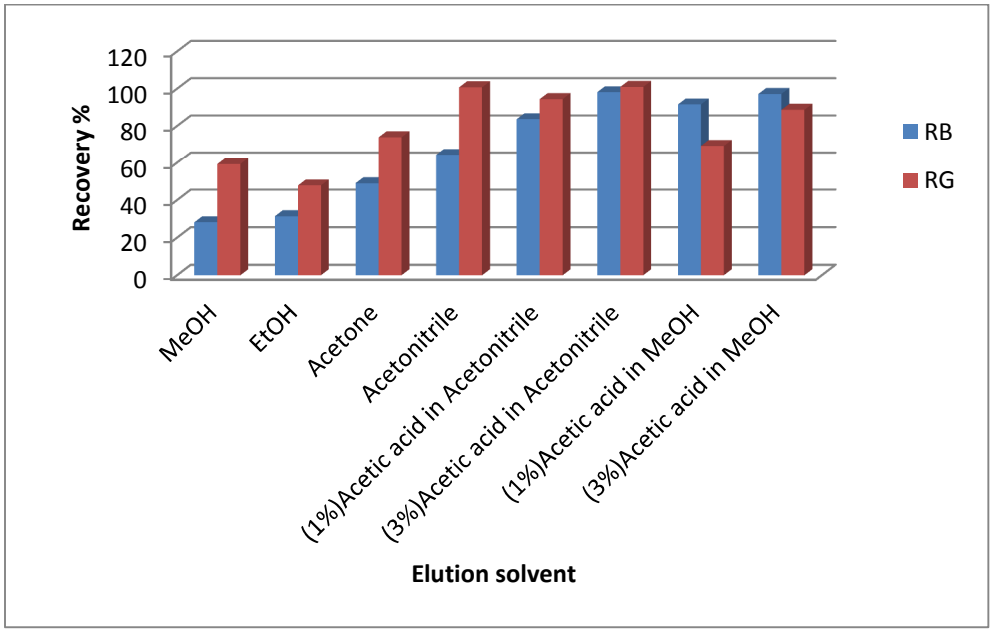

Figure S-7. Effect of different kinds of elution solvents on recovery of the dyes.

Table S-3. Main factors, symbols, levels and design matrix for simultaneous optimization of volume of elution solvent and amount of MHAMS-MIONPs.

Factor	Symbol	Level				
		-1.41	-1	0	1	1.41
Volume of elution solvent (mL)	X_1	0.59	1	2	3	3.41
Amount of MHAMS-MIONPs (mg)	X_2	40	50	75	100	110

Run	X_1	X_2	Multiplication of extraction recovery (MER)
1	-1	-1	0.606761201
2	-1	1	0.869403098
3	1	-1	0.798875698
4	1	1	0.96868209
5	-1.41	0	0.755060288
6	1.41	0	0.973098236
7	0	-1.41	0.587423586
8	0	1.41	0.977806491
9	0	0	0.958770709
10	0	0	0.979336438
11	0	0	0.935218214
12	0	0	0.962188511
13	0	0	0.927393491
14	0	0	0.943052642
15	0	0	0.950927361
16	0	0	0.954833938

Table S-4. ANOVA table for optimization of elution solvent volume and amount of MHAMS-MIONPs.

Source	Sum of Squares	df	Mean Square	F Value	p-value Prob > F	
Model	0.247081	5	0.049416	123.111	0.000000	significant
X'_1	0.044958	1	0.044958	168.203	0.000004	significant
$X'_1{}^2$	0.017435	1	0.017435	65.230	0.000086	significant
X'_2	0.121119	1	0.121119	453.148	0.000000	significant
$X'_2{}^2$	0.061218	1	0.061218	229.036	0.000001	significant
$X'_1X'_2$	0.002155	1	0.002155	8.061	0.025073	significant
Lack of Fit	0.002143	3	0.000714	2.673	0.128270	not significant
Pure Error	0.001871	7	0.000267			
Residual	0.004014	10				
Total SS	0.251095	15				

Table S-5. Tolerance limits of interfering species in the determination of 0.5 mg L^{-1} RB and RG.

Interference	Tolerance ratio (interfering agent/analyte (w/w))	Added as
Cations		
Na^+	4500	NaCl
K^+	4000	KCl
Mg^{2+}	2500	$MgCl_2$
Ca^{2+}	2500	$CaCl_2$
Fe^{3+}	1000	$FeCl_3.6H_2O$
Anions		
NO_3^-	8500	$NaNO_3$
CO_3^{2-}	4000	Na_2CO_3
PO_4^{3-}	3500	Na_3PO_4

Table S-6. Removal and determination of RB and RG in waste and environmental water samples.

Sample	Compound	Removal		Determination		
		Added (mg L^{-1})	RE% ± RSD%	Found	Added (mg L^{-1})	ER%± RSD%
MWW	RB	50	99.88 ± 0.16	Nd	0.01	93.97 ± 4.15
	RG	50	99.96 ± 0.15	Nd	0.01	92.25 ± 3.86
Waste water of the UA	RB	50	99.99 ± 0.15	Nd	0.01	95.16 ± 4.23
	RG	50	99.99 ± 0.18	Nd	0.01	96.38 ± 4.73
River water	RB	50	99.97 ± 0.16	Nd	0.01	94.39 ± 3.72
	RG	50	99.91 ± 0.16	Nd	0.01	92.48± 4.07

References

(S1) Bootz, A.; Vogel, V.; Schubert, D.; Kreuter, J. *Eur. J. Pharm. Biopharm.* **2004**, 57, 369-375.

(S2) Liu, X.; Zhang, H.; Chang, L.; Yu, B.; Liu, Q.; Wu, J.; Yuqing M.; Pei M.; Daidi F.; Fan, H. *Nanoscale Res. Lett.* **2015**, 10, 1-8.

(S3) Hall, J. B.; Dobrovolskaia, M. A.; Patri, A. K.; McNeil, S. E. *Nanomedicine-UK* **2007**, 2, 789-803.

(S4) Box, G. E.; Wilson, K. B. *J. Roy. Stat. Soc. B* **1951**, 13, 1-45.

(S5) Myers, R. H.; Montgomery, D. C.; Anderson-Cook, C. M. *Response surface methodology: process and product optimization using designed experiments*, John Wiley & Sons: New York, 2002.

(S6) Morgan, E. D. *Chemometrics: experimental design*, Wiley: New York, 1995.

(S7) Prosser, A. J.; Franses, E. I. *Langmuir* **2002**, 18, 9234-9242.

(S8) Majoube, M.; Henry, M. *Spectrochim. Acta A-M* **1991**, 47, 1459-1466.